Neoadjuvant STING Activation, Extended Half-life IL2, and Checkpoint Blockade Promote Metastasis Clearance via Sustained NK-cell Activation

Lauren E. Milling[1,2], Daniel Garafola[2], Yash Agarwal[1,2], Shengwei Wu[2], Ayush Thomas[2], Nathan Donahue[2], Josetta Adams[2], Nikki Thai[2], Heikyung Suh[2], and Darrell J. Irvine[1,2,3,4,5]

ABSTRACT

Combination immunotherapy treatments that recruit both innate and adaptive immunity have the potential to increase cancer response rates by engaging a more complete repertoire of effector mechanisms. Here, we combined intratumoral STimulator of INterferon Genes (STING) agonist therapy with systemically injected extended half-life IL2 and anti–PD-1 checkpoint blockade (hereafter CIP therapy) to drive innate and adaptive antitumor immunity in models of triple-negative breast cancer. Unlike treatment with the individual components, this trivalent immunotherapy halted primary tumor progression and led to long-term remission for a majority of animals in two spontaneously metastasizing orthotopic breast tumor models, though only as a neoadjuvant therapy but not adjuvant therapy. CIP therapy induced antitumor T-cell responses, but protection from metastatic relapse depended on natural killer (NK) cells. The combination of STING agonists with IL2/anti–PD-1 synergized to stimulate sustained granzyme and cytokine expression by lung-infiltrating NK cells. Type I IFNs generated as a result of STING agonism, combined with IL2, acted in a positive-feedback loop by enhancing the expression of IFNAR-1 and CD25 on lung NK cells. These results suggest that NK cells can be therapeutically targeted to effectively eliminate tumor metastases.

See related Spotlight by Demaria, p. 3.

Introduction

Combination treatments driving synergistic pathways of immunity against tumors may enhance cancer immunotherapy outcomes. Therapies promoting innate and adaptive immune responses in tandem may be of particular value by leveraging the full armamentarium of the immune response (1, 2). For example, natural killer (NK) cells have been shown to engage in cross-talk with dendritic cells (DC) through tumor-specific mAbs; antibodies bound to tumor cells trigger antibody-dependent cellular cytotoxicity from NK cells followed by immune complex uptake by DCs for T-cell priming (3, 4). In addition to direct cytolytic effects, NK cells secrete proinflammatory cytokines such as IFNγ and TNFα, which induce antiproliferative and antiangiogenic effects within the tumor microenvironment and further stimulate T-cell cytotoxicity (5).

We previously reported on a combination therapy, AIPV, comprised of a peptide vaccine, tumor-specific antibody, extended half-life IL2 (an albumin-IL2 fusion, Alb-IL2), and anti–PD-1 checkpoint blockade (6). Alb-IL2 has a terminal half-life around 50 hours in circulation (7). Weekly dosing with this quaternary combination leads to rejection of large, established tumors and generates long-lived T-cell memory responses in several syngeneic cancer models, including a genetically engineered model of melanoma. These therapeutic responses are dependent on multiple innate immune cell populations, including NK cells, macrophages, and neutrophils. However, the use of two tumor antigen–specific components (vaccine and antibody) makes AIPV therapy challenging to translate to clinical testing. We thus sought to identify a simplified, tumor-agnostic combination treatment capable of similarly potentiating innate and adaptive immune responses in tandem.

The antitumor antibody and vaccine components of AIPV drive initial rapid tumor cell killing and antitumor T-cell priming, respectively. We hypothesized that intratumoral treatment with ligands for STimulator of INterferon Genes (STING) could replace these functions. STING signaling has been implicated in the generation of tumor debris through immunogenic cell death (8–10). Following tumor antigen release, STING signaling can trigger DC activation and cross-presentation (10). Exploiting this effect, STING agonists have been explored as vaccine adjuvants for improving T-cell priming (11, 12). Notably, STING expression in host cells, rather than cancer cells, is essential for the generation of tumor-reactive cytotoxic T cells in many models of cancer treatment (13). Furthermore, STING activation also stimulates innate immunity, and STING agonists have been explored for their ability to stimulate natural killer (NK) cells in $CD8^+$ T-cell–resistant preclinical tumor models (14, 15). *Tmem173* (STING) gene expression is also associated with tumoricidal capacity of neutrophils in breast cancer (16).

Encouraged by the precedent of STING agonists serving as pleiotropic modulators of both adaptive and innate immune cells, we explored the use of intratumorally injected STING agonists (cyclic dinucleotides, C) as a means to promote antitumor immunity in

[1]Department of Biological Engineering, Massachusetts Institute of Technology, Cambridge, Massachusetts. [2]Koch Institute for Integrative Cancer Research, Massachusetts Institute of Technology, Cambridge, Massachusetts. [3]Ragon Institute of Massachusetts General Hospital, Massachusetts Institute of Technology and Harvard University, Cambridge, Massachusetts. [4]Department of Materials Science and Engineering, Massachusetts Institute of Technology, Cambridge, Massachusetts. [5]Howard Hughes Medical Institute, Chevy Chase, Maryland.

Corresponding Author: Darrell J. Irvine, Biological Engineering, Massachusetts Institute of Technology, MIT Room 76-261, Cambridge, MA 02139. Phone: 617-452-4174; E-mail: djirvine@mit.edu

Cancer Immunol Res 2022;10:26–39

doi: 10.1158/2326-6066.CIR-21-0247

concert with systemic administration of Alb-IL2 (I) and anti–PD-1 (P) in orthotopic mouse models of triple-negative breast cancer. Naturally metastatic syngeneic breast tumor models allow for profiling the immune response directed against primary tumors as well as distant metastases, from which patients with triple-negative breast cancer are more likely to suffer than other patients with breast cancer (17). Although CIP therapy elicited $CD8^+$ T-cell priming, we found that in the setting of neoadjuvant treatment, this combination therapy also triggered activation of NK cells that mediated protection from metastases in the lungs. Type I IFNs elicited from STING activation in the primary tumor, together with IL2, drove sustained proliferation and expression of effector molecules, including granzyme B, IFNγ, TNFα, perforin, and NKG2D in lung NK cells. Hence, this tumor-agnostic immunotherapy elicited combined innate and adaptive immune responses, with the innate response playing an important role in protection from metastases in multiple models of breast cancer.

Materials and Methods

Mice

BALB/c, C57BL/6, NOD.Cg-Prkdc^{scid}/J (NOD SCID), NOD.Cg-Prkdc^{scid} Il2rg^{tm1Wjl}/SzJ (NSG), and B6.129-Ifnb1^{tm1Lky}/J (IFNβ reporter) mice were purchased from The Jackson Laboratory or bred in-house. Mice were used in studies when 7 to 10 weeks old. All animal work was conducted under the approval of the Massachusetts Institute of Technology (MIT) Committee on Animal Care and the Division of Comparative Medicine in accordance with federal, state, and local guidelines.

Cell culture

4T1 cells were purchased from ATCC (CRL-2539, ATCC) in 2011. 4T1-GFP-Luc (4T1-Luc) cells were generated by transduction of the 4T1 cell line with pGreenFire lentiviral vector (System Biosciences). Cells were cultured in RPMI1640 Medium supplemented with 10% FBS, penicillin (100 U/mL), and streptomycin (100 μg/mL). E0771 cells were a gift from Mikala Egeblad, received in 2020 (Cold Spring Harbor). E0771 cells were cultured in DMEM supplemented with 10% FBS, penicillin (100 U/mL), and streptomycin (100 μg/mL). HEK293 cells (R790-07, Invitrogen), acquired in 2017, were cultured in Freestyle Media (12338-018, Life Technologies). All cells were maintained at 37°C and 5% CO_2 and passaged fewer than five times. All cell lines tested negative for *Mycoplasma* and rodent pathogens quinquennially. Cell line authentication was not routinely performed.

Antibodies and reagents

Purified anti-mouse PD-1 mAb (RMP1–14), anti-mouse CD8 (2.43), anti-mouse Ly6G (1A8), anti-mouse CD4 (GK1.5), anti-mouse NK1.1 (PK136), anti-mouse IFNAR-1 (MAR1–5A3), control rat IgG2a (2A3), and control rat IgG2b (LTF2) were purchased from BioXCell. Anti–PD-1 was administered intraperitoneally at 200 μg per dose on the indicated schedules. Cellular depletions were conducted by administering 400 μg of depleting antibody (2.43, 1A8, GK1.5, PK136) or isotype control (2A3, LTF2) intraperitoneally beginning 1 day prior to initiation of therapy then every 3 days for a total of seven doses. Anti-asialoGM1 (Wako Chemicals) was administered intraperitoneally in 50 μL doses for NK-cell depletion on the same schedule. IFNAR-1 blocking was accomplished by administering 500 μg of MAR1-5A3 antibody intraperitoneally 48 and 24 hours prior to commencement of therapy and dosed every 3 days.

STING agonist 2′3′ c-di-AM(PS)$_2$ (R_p,R_p) (CDN, tlrl-nacda2r, Invivogen) was injected intratumorally (i.tu.) at 30 μg per dose in a 30 μL volume on the indicated schedules.

Albumin-IL2 fusion (Alb-IL2) protein was produced in HEK293 cells as described previously (7). Alb-IL2 was administered intraperitoneally at 30 μg (6 μg molar equivalent of IL2) per dose. For *in vitro* studies, murine IFN alpha-A and murine IFN beta-1 with C-terminal His-tags were cloned into the gWiz expression vector (Gelantis). HEK293 cells were transfected with plasmid DNA using OptiPRO serum-free media and polyethylenimine. IFN was purified from the supernatant using TALON metal affinity resin (Takara Bio), buffer exchanged into PBS, and sterile filtered.

Orthotopic, tumor induction, and surgical resection

For orthotopic tumor studies, 5×10^5 4T1-Luc tumor cells were inoculated into the fourth mammary fat pad of BALB/c, NOD SCID, or NSG mice, and 5×10^5 E0771 cells were inoculated into the fourth mammary fat pad of C57BL/6 mice. Treatment was administered according to the referenced timelines, generally beginning when tumors reached 50 to 100 mm^3 ($0.5^*L^*(W^2)$). Nine days after the start of treatment, mice were anaesthetized with isoflurane and provided preoperative subcutaneous sustained-release buprenorphine (1 mg/kg, ZooPharm) and meloxicam (5 mg/kg). The primary tumor and draining inguinal lymph node were surgically removed and the wound was closed with surgical clips. Inguinal lymph nodes were removed because of primary tumors frequently growing around the node; therefore, the inguinal lymph node was removed in all mice. Meloxicam (5 mg/kg) was dosed every 24 hours for 3 days postoperatively. Mice were then monitored every other day and euthanized if signs of distress, >20% body weight loss, or poor body condition were observed.

Bioluminescence imaging

4T1-Luc tumor–bearing mice were monitored postoperatively for development of metastases using bioluminescence imaging beginning 1 week after surgical resection of the primary tumor. Animals were injected intraperitoneally with 150 mg/kg sterile filtered D-Luciferin (PerkinElmer) in 200 μL of sterile PBS. Animals were imaged 10 minutes after D-Luciferin injection using the IVIS Spectrum Imagining System 100 (IVIS, Xenogen).

Aspartate aminotransferase assay and alanine transaminase assay

4T1-Luc tumor–bearing mice were treated with 30 μg CDN i.tu., 30 μg Alb-IL2 i.p., and 200 μg anti–PD-1 i.p., or listed subsets beginning 8 days after tumor inoculation. A total of 50 μL of blood was sampled 24, 48, and 72 hours after treatment initiation and assayed for aspartate aminotransferase (AST) and alanine aminotransferase (ALT) activity according to the manufacturer's protocol (Sigma).

Evans blue pulmonary vessel permeability assay

4T1-Luc tumor–bearing mice were treated with 30 μg CDN i.tu., 30 μg Alb-IL2 i.p., and 200 μg anti–PD-1 i.p., or listed subsets beginning 8 days after tumor inoculation. A total of 100 μg recombinant human IL2 (Peprotech) was administered intraperitoneally every 12 hours for three doses as a positive control. A total of 24 hours after one round of treatment, animals were injected intravenously with 200 μL of 0.5% Evans blue dye. Lungs were harvested 30 minutes after dye injection, weighed, and placed in 500 μL formamide. Lung samples were incubated in formamide at 37°C shaking for 24 hours before OD 620 was measured and quantified against a standard curve.

Metastasis colony formation assay

Micrometastases in the 4T1-Luc tumor model were quantified in the lungs and axillary lymph nodes by a 6-thioguanine selection assay as described previously (18). Briefly, lungs and lymph nodes were isolated at indicated times post tumor inoculation. Lungs were digested at 4°C for 75 minutes in 1 mg/mL Collagenase IV (Gibco) and 6 U/mL elastase (Worthington Biochemical), filtered through a 70 μm nylon cell strainer, and cultured in 10 cm dishes in selection media of Iscove's Modified Dulbecco's Medium supplemented with 10% FBS, 1× antibiotic-antimycotic (Life Technologies), and 60 μmol/L 6-thioguanine (Sigma). Lymph nodes were mechanically disrupted using a mortar and pestle (Kimble Biomasher) and cultured in 6-well plates in selection media. After 14 days in culture at 37°C and 5% CO_2 without disruption, colonies were fixed in methanol, developed using 0.03% (w/v) methylene blue (Sigma) in water, and colonies manually quantified.

Flow cytometry analysis

Antibodies to CD45 (30-F11), CD45.2 (104), CD3ε (145-2C11), CD8α (53-6.7), CD4 (RM4-5), CD25 (PC61), NKp46 (29A1.4), NK1.1 (PK136), Ly6C (HK1.4), Ly6G (1A8), CD11c (N418), CD11b (M1/70), I-A/I-E (M5/114.15.2), Granzyme B (GB11), IFNγ (XMG1.2), PD-1 (29F.1A12), Perforin (S16009B), TNFα (MP6-XT22), IL2 (JES6–5H4), CD69 (H1.2F3), IFNAR (MAR1–5A3), NKG2D (CX6), DNAM-1 (10E5), FasL (MFL3), and mTRAIL (N2B2) were purchased from BioLegend. Antibodies to CD45 (30–F11) and Ki67 (B56) were purchased from BD Biosciences. FoxP3 (FJK-16s) antibody was purchased from Thermo Fisher Scientific. Gp70 tetramer (T-Select H-2L^d MuLV gp70 Tetramer-SPSYVYHQF-PE) was purchased from MBL. Tetramer staining was performed in buffer containing 50 nmol/L dasatinib. Viability was assessed using LIVE/DEAD Fixable Aqua (Life Technologies) for tumor, lung, and spleen samples or using DAPI for tetramer staining of blood samples. FoxP3 staining and Ki67 staining were performed using the FoxP3 Transcription Factor Buffer Set (eBioscience).

Immune cell infiltrates of tumors, lungs, and spleens were analyzed as described previously (19); briefly, organs were harvested day 1, 3, or 6 after the start of treatment. Before tissue harvest, mice were injected 2 minutes prior to euthanasia retro-orbitally with an APC-Cy7 conjugated anti-CD45.2 antibody to label hematopoietic cells in the circulation but not the lung parenchyma. Tumors and lungs were cut into 1 to 2 mm size pieces and digested at 37°C for 30 minutes in the following enzyme solutions. 4T1-Luc: 10 mg/mL collagenase I (Gibco) and 40 U/mL DNase I (Roche); E0771 and lungs: 125 U/mL collagenase IV (Gibco) and 40 U/mL DNase I in 1× HBSS. The digested tissues were then passed through a 70 μm nylon cell strainer. Spleens were mechanically disrupted through 70 μm nylon cell strainers. All tissues were pelleted to remove digestion buffer, red blood cells were lysed in ACK lysis buffer (Gibco), and samples were washed in buffer containing 2% (w/v) BSA and 5 mmol/L EDTA (staining buffer). For intracellular cytokine/granule staining of tissue infiltrating cells, digested and lysed tissue samples were resuspended in staining buffer containing 1× brefeldin A (BioLegend) for at least 1 hour prior to staining. Cells were analyzed using a BD FACS LSR II, BD FACS LSR Fortessa, or BD FACS Canto flow cytometers. Data were analyzed in FlowJo.

Fluorescent CDN uptake

4T1-Luc tumor–bearing mice were treated intratumorally with a mixture of 30 μg 2′3′ c-di-AM(PS)$_2$ and 5 nmoles sulfo-Cy5 labeled 2′3′ c-GAMP (Biolog) in 30 μL. sulfo-Cy5 2′3′ c-GAMP was selected because of lack of commercially available labeled 2′3′ c-di-AM(PS)$_2$. Tumors, blood, and lungs were collected 2, 6, and 24 hours after injection and processed as described above. Cy5 signal was analyzed by flow cytometry using a BD FACS LSR Fortessa.

IFNβ reporter assay

A total of 5×10^5 E0771 cells were inoculated into the fourth mammary fat pad of IFNβ reporter mice. Two weeks after tumor inoculation, mice received one dose of CDN (30 μg i.tu.), Alb-IL2 (30 μg i.p.), and anti–PD-1 (200 μg i.p.). A total of 24 hours after treatment tumors and lungs were processed for flow cytometry according to the protocol above. eYFP signal was analyzed using a BD FACS LSR Fortessa.

Serum cytokine analysis

Serum samples were collected from 4T1-Luc tumor–bearing mice by retro-orbital bleed 6 and 24 hours after one dose of combination immunotherapy and frozen at −20°C until analysis. Samples were diluted 1:1 with Assay Buffer and assayed using the LEGENDplex mouse antivirus response panel (BioLegend) according to manufacturer's instructions. The cytometric bead array readout was performed using a BD FACS LSR Fortessa cytometer and analyzed using LEGENDplex v8.0 software.

NK-cell isolation and *in vitro* stimulation

For *in vitro* stimulation assays, NK cells were isolated from spleens of 7- to 10-week-old Balb/c mice using an EasySep Mouse NK cell Isolation Kit (STEMCELL) according to the manufacturer's instructions. Cells were seeded at 50,000 NK cells per well in RPMI1640 with 10% FBS, 100 U/mL penicillin, 100 μg/mL streptomycin, 1× minimum essential medium non-essential amino acids (Gibco), and 1 mmol/L sodium pyruvate (Gibco). Alb-IL2, IFNβ, and IFNα were added in complete medium as indicated. Cells were incubated at 37°C and 5% CO_2 and stained with antibodies for flow cytometry 24 hours after stimulation unless indicated otherwise.

Statistical analysis

Statistics were performed using Prism (GraphPad). Statistical methods were not used to determine sample size, but sample numbers were chosen on the basis of estimates from pilot studies and published results, such that appropriate statistical tests would yield statistically significant results. For survival studies, log-rank (Mantel–Cox) tests were used. For immune cell infiltration studies, NK functional markers analyzed at multiple time points, and serum cytokine analysis two-way ANOVA tests were used followed by Dunnett multiple comparisons test versus untreated controls. For IFNAR blockade lung analysis, two-way ANOVA tests were used followed by Tukey multiple comparisons test. Unpaired two-tailed Student *t* test was utilized for analysis of NK functional markers induced by CIP versus untreated controls at a single time point. Significance is indicated as follows: *, $P < 0.05$; **, $P < 0.01$; ***, $P < 0.001$; ****, $P < 0.0001$. The *n* values and specific statistical methods are indicated in figure legends.

Results

Neoadjuvant CIP therapy promotes primary tumor regression and inhibits metastasis

We first explored combinations of cyclic dinucleotide (CDN) STING agonists, extended half-life Alb-IL2, and anti–PD-1 checkpoint blockade in a neoadjuvant model of triple-negative breast cancer.

Primary tumors were established by injection of 4T1-Luciferase cells into the mammary fat pad of female Balb/c mice. When tumors reached approximately 100 mm^3 in volume (8 days after inoculation) animals were treated with three doses of CDN alone every 3 days, two doses of Alb-IL2 and anti–PD-1 given 6 days apart, or the combination of all three agents, followed by surgical resection of tumors 9 days after start of treatment (CIP therapy; **Fig. 1A**). Intratumoral CDN monotherapy or the systemic Alb-IL2 and anti–PD-1 combination led to moderate primary tumor growth delay compared with untreated controls, but the triple combination halted primary tumor progression (**Fig. 1B**). Following tumor resection, untreated control animals succumbed to metastases with a median survival of 38 days. Treatment with CDN alone or the dual combination of IP resulted in median survival times of 44.5 and 47 days and long-term survival in 20% and 10% of mice, respectively. In contrast, CIP treatment increased the long-term survival rate to 60% (**Fig. 1C**). This enhancement in efficacy required all three components, as monotherapy or pairs of these agents were significantly less effective (Supplementary Fig. S1A). The combination treatment was well tolerated, with mice receiving CIP experiencing transient weight loss that recovered prior to surgery (Supplementary Fig. S1B). In addition, liver enzymes AST and ALT were elevated briefly following CIP treatment but returned to baseline by 72 hours after treatment (Supplementary Fig. S1C and S1D). Clinical use of recombinant IL2 is hindered by dose-limiting toxicities including increased lung vasculature permeability mediated by innate immune cell–induced damage to endothelial cells (20, 21). To assess the risk of enhanced vascular leak syndrome when combining Alb-IL2 with anti–PD-1 and STING agonist treatment, we evaluated alterations in lung vessel permeability by Evans Blue dye uptake. Although the lungs of animals receiving CIP treatment exhibited an approximately 75% increased uptake of intravenous administered Evans blue compared with untreated or Alb-IL2–treated controls, this increased permeability was still only 52% of that induced by traditional

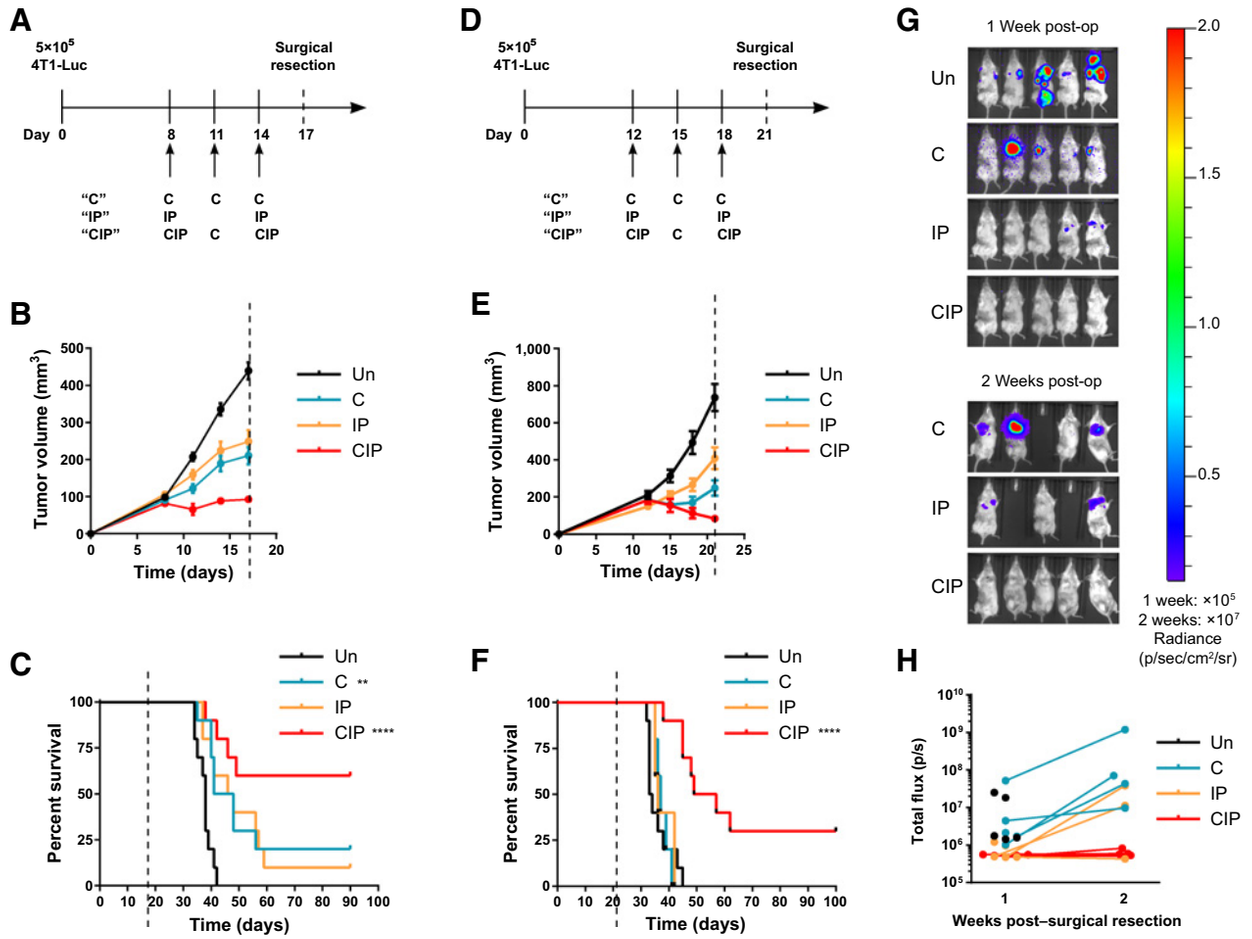

Figure 1.

Combination of neoadjuvant CDN STING agonist therapy with systemic Alb-IL2 and anti–PD-1 improves survival in an orthotopic breast tumor model. **A–C,** Balb/c mice ($n = 10$ animals/group) were inoculated with 4T1-Luc cells in the mammary fat pad and then treated with 30 μg CDN 2′3′-cdiAM(PS)$_2$ (i.tu.), 30 μg Alb-IL2 (i.p.), and 200 μg anti–PD-1 (i.p.) or subcombinations of these agents as indicated, followed by surgical resection of the tumor. Shown are the treatment schedules (**A**), mean tumor volume (**B**), and survival curves (**C**). **D–H,** Neoadjuvant therapy as in **A**, with treatment commencing 12 days after tumor inoculation. Shown are treatment schedules (**D**), mean tumor volume (**E**), survival curves (**F**), representative bioluminescence images (**G**), and luminescence quantification (**H**). Data compiled from two independent experiments. Data represent the mean ± SEM. **, $P < 0.01$; ****, $P < 0.0001$; versus untreated by log-rank (Mantel–Cox) test.

high-dose IL2 therapy (Supplementary Fig. S1E). Altogether, this treatment appeared to be safe and effective as a neoadjuvant therapy.

Analysis of micrometastases with a colony outgrowth assay on lung tissues at various time points after primary tumor inoculation pinpointed metastatic seeding of the draining axillary lymph node and lungs between 10 and 14 days after mammary fat pad injection (Supplementary Fig. S2A and S2B). To evaluate whether CIP could eliminate tumors in mice with definitively established micrometastases, we delayed the start of treatment until day 12 after tumor cell inoculation, when primary tumors were approximately 200 mm^3 (**Fig. 1D**). In this setting, treatment with CDN or Alb-IL2/anti–PD-1 delayed primary tumor growth, but all animals succumbed to metastatic disease following primary tumor resection at a rate indistinguishable from untreated controls (**Fig. 1E** and **F**). The triple combination, however, resulted in regression of primary tumors, and following surgery, 30% of mice survived long term (**Fig. 1E** and **F**). Postresection bioluminescence imaging revealed expansion of metastases distal to the primary tumor site as early as 1 week after resection in untreated, CDN monotherapy, and IP dual therapy groups (**Fig. 1G** and **H**). We also tested this treatment in C57Bl/6 mice, orthotopically implanting E0771 breast tumors. In this model, neoadjuvant CIP was similarly well tolerated and led to 100% survival following primary tumor resection, whereas only 23% of mice left untreated following resection survived longer than 100 days, with a median survival time of 53 days (Supplementary Fig. S3A–S3D).

Given the efficacy of CIP, we next examined whether neoadjuvant or adjuvant administration was more effective in the 4T1-Luc model. To initiate adjuvant therapy at a time point before an overwhelming metastatic burden was established, we compared neoadjuvant treatment beginning on day 6 when tumors were approximately 40 mm^3 against treatment beginning 3 days after surgery (**Fig. 2A**). Neoadjuvant CIP resulted in 90% overall survival, whereas only 1 of 10 mice survived following adjuvant immunotherapy (**Fig. 2B**). Next, we sought to assess the importance of surgical resection of the primary

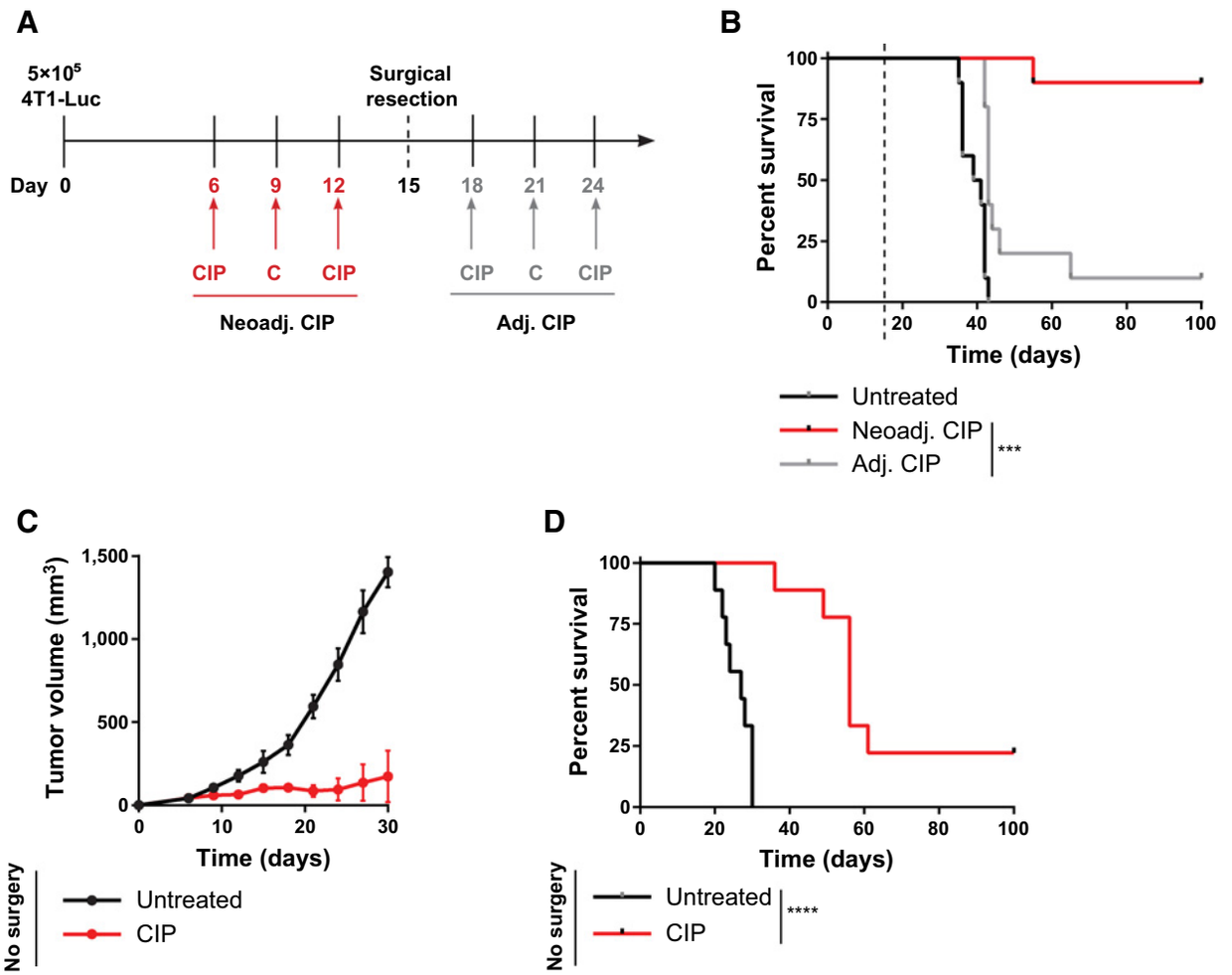

Figure 2.

Maximal efficacy of CIP immunotherapy requires neoadjuvant treatment scheduling and surgical resection of the primary tumor. **A,** Timeline and components of treatment consisting of 30 μg CDN 2′3′-cdiAM(PS)2 (i.tu.), 30 μg Alb-IL2 (i.p.), and 200 μg anti–PD-1 (i.p.). Surgical removal of primary tumor was conducted on day 15. **B,** Survival curves for mice treated as in **A**. In **B**, $n = 10$ Balb/c mice per group, and data were compiled from two independent experiments. Mean tumor volume (**C**) and survival over time (**D**) for mice treated as in **A** without surgical resection of the primary tumor. In **C** and **D**, $n = 9$ Balb/c mice per group. Data in **C** represent mean ± SEM. ***, $P < 0.001$; ****, $P < 0.0001$; versus neoadj. log-rank (Mantel–Cox) test.

tumor. CIP therapy administered beginning on day 6 arrested primary tumor growth up to 30 days after inoculation, but most primary tumors progressed by day 40, leading to poor overall survival (**Fig. 2C** and **D**; Supplementary Fig. S4A). When treatment commenced 8 days after tumor inoculation, in the absence of surgical resection, both CI and CIP treatment yielded tumor clearance in about 40% of mice (Supplementary Fig. S4B–S4D). The greater efficacy of CIP over CI treatment in the setting of neoadjuvant therapy, but not in the absence of surgery, suggests the triple combination enhances immune control of residual metastases, but addition of checkpoint blockade is not important for control of the primary tumor. Altogether, treatment in the neoadjuvant setting with surgical intervention maximizes the therapeutic benefit of CIP combination therapy.

CIP treatment induces changes in immune cell infiltration at the primary tumor and lungs

As STING agonism, IL2, and checkpoint blockade have each been documented to engage both innate and adaptive immune cells, we profiled immune cell infiltration in primary tumors and the lungs as the predominant site of metastasis (Supplementary Fig. S5A; refs. 18, 22–24). Within primary 4T1 tumors, treatments containing Alb-IL2 enhanced infiltration of $CD8^+$ T cells (**Fig. 3A**). Following monotherapy treatment, $CD4^+$ effector T cells and regulatory T cell (Treg) numbers declined from 3 to 6 days at the primary tumor, but CIP led to sustained numbers (**Fig. 3B** and **C**). Despite increases in Tregs within the primary tumor, Alb-IL2 monotherapy drove increased $CD8^+$/Treg ratios compared with untreated controls, and CIP trended toward an increased ratio (**Fig. 3D**). Both CDN monotherapy and the triple combination treatment also elicited significantly increased primary tumor infiltration of $CD3^-NKp46^+$ NK cells as early as 3 days following the first dose of treatment (**Fig. 3E**). Absolute NK-cell numbers in these two groups continued to rise within primary tumors, reaching a peak of around 10-fold over untreated controls 6 days after treatment. Cohorts receiving intratumoral CDN or CIP exhibited increased primary tumor neutrophil counts (**Fig. 3F**).

In the lungs of both 4T1-Luc and E0771 tumor–bearing mice, $CD8^+$, $CD4^+$, and Treg infiltration was elevated 3 days after commencement of treatment with IP. In both models, CIP similarly increased $CD8^+$ and Treg infiltration in the lungs, but $CD4^+$ effector cells were less abundant than post-IP treatment (**Fig. 3G–I**; Supplementary Fig. S6A–S6C). At 3 days after treatment, T-cell counts in the spleen were not significantly different from controls, but $CD8^+$ T cells and Tregs showed a transient expansion in the blood at 3 days post CIP, followed by a contraction at day 6 (Supplementary Fig. S7A–S7F). High numbers of NK cells were present in the lungs of tumor-bearing mice irrespective of treatment condition, peaking at day 3 but remaining high 6 days after treatment (**Fig. 3J**; Supplementary Fig. S6D). In contrast, there was no increase in total NK-cell count within the spleen nor blood following immunotherapy administration (Supplementary Fig. S7G and S7H). Although neutrophils increased in primary tumors with time, they were depleted from the lung, spleen, and blood following CIP therapy (**Fig. 3K**; Supplementary Fig. S7I and S7J). Classical $CD11b^+MHC^{low}Ly6G^-Ly6C^{hi}$ inflammatory monocytes showed no treatment-induced changes in infiltration in the lungs, spleen, and blood (Supplementary Figs. S5B, and S7K and S7L); however, nonclassical patrolling monocytes ($CD11b^+MHC^{low}Ly6G^-Ly6C^{low}$) transiently infiltrated the lungs in CIP-treated mice (Supplementary Fig. S5C). Overall, CIP treatment altered both adaptive and innate leukocyte proportions within intratumorally injected and noninjected tissues.

Long-term survival following CIP therapy is independent of T cells and dependent on NK cells

To determine which immune cells govern therapeutic responses to CIP treatment, we performed cellular depletion studies in the 4T1 model (Supplementary Fig. S8A). Depletion of neutrophils, $CD8^+$ T cells, or $CD4^+$ T cells did not impact primary tumor progression nor survival during CIP treatment (**Fig. 4A–C**; Supplementary Fig. S8B–S8D). In contrast, an approximate 50% reduction in survival rate was observed when NK cells were depleted (**Fig. 4D**; Supplementary Fig. S8E).

To further examine the role of NK cells in the response to CIP, we treated 4T1 tumors in NOD.Cg-Prkdc^{scid}/J (NOD SCID) mice, which lack functional B and T cells (25), and NOD.Cg-Prkdc^{scid} Il2rg^{tm1Wjl}/SzJ (NSG) mice, which lack B and T cells as well as functional, mature NK cells (26). CIP therapy delayed primary tumor growth in NOD SCID animals, though to a lesser degree than Balb/c mice; tumor progression was even less impacted in NSG mice (**Fig. 4E**). Following surgical resection, no significant survival benefit was detected for CIP-treated NSG mice compared with untreated controls (**Fig. 4F**). In contrast, 78% of treated Balb/c mice and 56% of treated NOD SCID mice survived greater than 90 days, suggesting that NK cells play an important role in preventing metastatic disease (**Fig. 4F**).

Despite the maintenance of therapeutic response in the absence of $CD8^+$ T cells, several lines of evidence suggested that CIP treatment induced an adaptive immune response. Analysis of peripheral blood 2 weeks after tumor resection revealed increased frequencies of $CD8^+$ T cells specific for the endogenous retroviral antigen gp70 expressed by 4T1 cells (27) following CIP therapy (Supplementary Fig. S9A). Mice surviving greater than 90 days following CIP neoadjuvant therapy were rechallenged with 4T1-Luc tumor cells in the hind flank. Animals that had received neoadjuvant CDN monotherapy exhibited tumor outgrowth on rechallenge indistinguishable from naïve mice, but animals that had received neoadjuvant CIP or subcombinations of the triple therapy exhibited significantly delayed secondary tumor growth (Supplementary Fig. S9B). Two weeks after rechallenge, animals previously treated with neoadjuvant CIP showed substantial expansion of gp70-specific T cells in the blood (Supplementary Fig. S9C). Depletion of $CD8^+$ T cells during rechallenge resulted in a significant acceleration of rechallenge tumor growth in mice previously treated with CIP compared with controls (Supplementary Fig. S9D). During primary tumor challenge, activated ($CD44^+IFN\gamma^+$) $CD8^+$ T cells expanded by percentage and number in the lungs (Supplementary Fig. S9E). Finally, expression of PD-1 and Tim-3 by lung $CD44^+$ or $CD44^+IFN\gamma^+$ T cells was largely unchanged in treated versus untreated conditions (Supplementary Fig. S9F and S9G). Thus, although T cells do not play a role in protection from metastases in this model, antitumor T-cell responses are induced by CIP treatment.

NK-cell activation is sustained by CIP therapy

We next examined functional markers expressed by the lung-infiltrating NK-cell population following treatment. CIP therapy led to substantial increases in the fraction of NK cells expressing the cytotoxic granule components granzyme B and perforin; cytokines TNFα, IFNγ, and IL2; early activation marker CD69; proliferation marker Ki67; and the exhaustion marker PD-1 (**Fig. 5A**). We next sought to examine the behavior of granzyme B and PD-1 over time and to dissect the impact of individual components of the combination therapy. CIP induced an increase in NK-cell granzyme B expression in the lungs significantly higher than that elicited by CDN or Alb-IL2

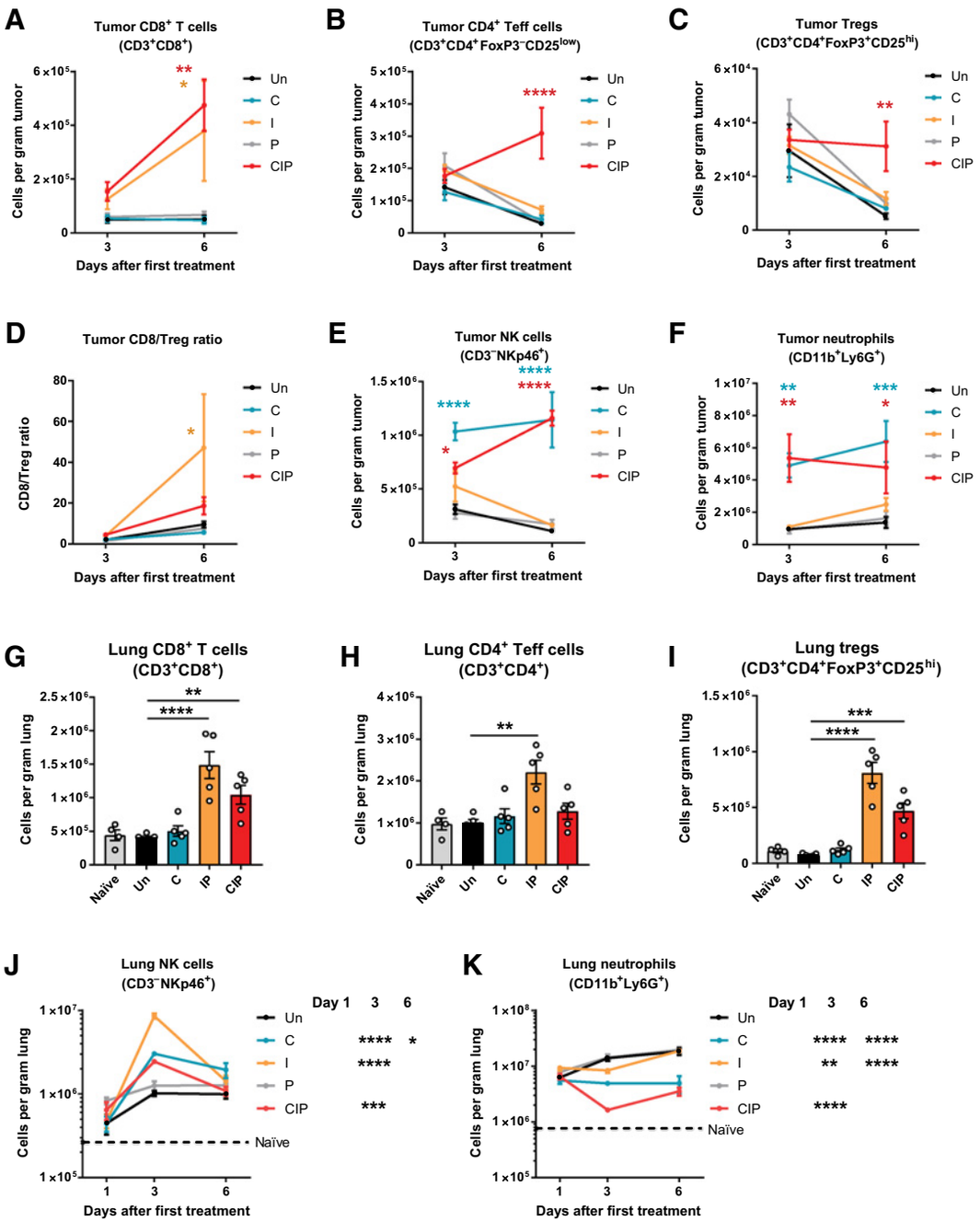

Figure 3.

CIP immunotherapy alters adaptive and innate immune cell infiltration in primary tumors and lungs. **A–K,** Mice were inoculated with 5×10^5 4T1-Luc tumor cells in the mammary fat pad and treated with CIP or the individual agents when tumors reached 50 to 100 mm^3. Age-matched naïve, non–tumor-bearing mice were used as controls. Tumors (**A–F**) and lungs (**G–K**) were isolated 1, 3, or 6 days after initiation of treatment, as indicated, and cells quantified by flow cytometry. Shown are tumor-infiltrating $CD8^+$ T cells (**A**), $CD4^+$ effector T (T_{eff}) cells (**B**), Tregs (**C**), CD8/Treg ratio (**D**), NK cells (**E**), and neutrophils (**F**); lung-infiltrating $CD8^+$ T cells (**G**), $CD4^+$ T_{eff} cells (**H**), and Tregs (**I**) from 3 days after treatment; and lung-infiltrating NK cells (**J**) and neutrophils (**K**) from 1, 3, and 6 days after treatment. Data shown are mean ± SEM and are representative of at least two independent experiments ($n = 4$ naïve or 5 tumor-bearing mice per group per time point). *, $P < 0.05$; **, $P < 0.01$; ***, $P < 0.001$; ****, $P < 0.0001$ versus untreated at each time point by two-way ANOVA followed by Dunnett multiple comparisons test.

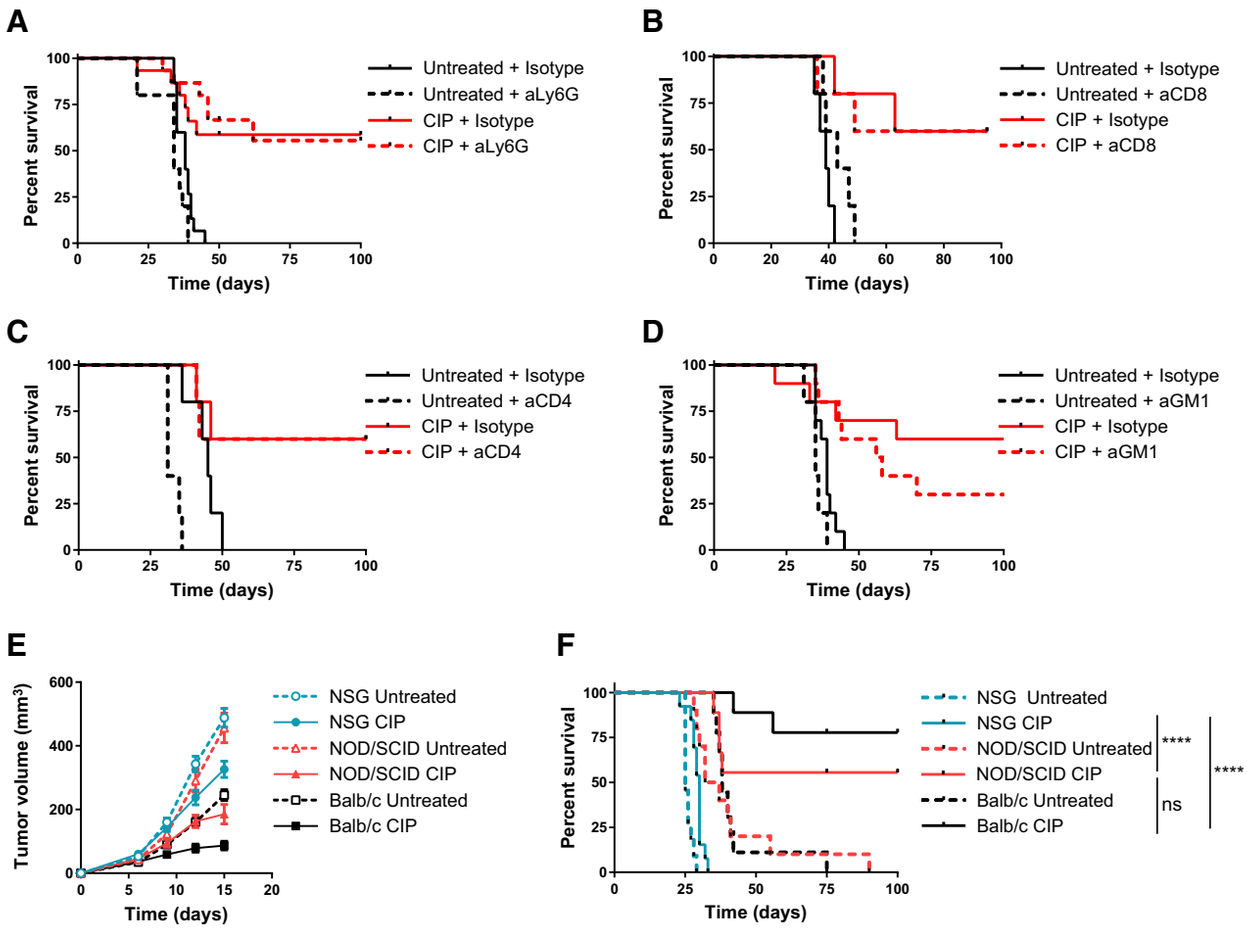

Figure 4.

Efficacy of CIP therapy is independent of T cells and neutrophils but dependent on NK cells. **A–D,** Balb/c mice bearing orthotopic 4T1-Luc tumors were treated as in **Fig. 1A** in the presence of depleting antibodies specific for the indicated surface markers or isotype controls. Shown is overall survival following depletion of neutrophils (**A**), $CD8^+$ T cells (**B**), $CD4^+$ T cells (**C**), or NK cells (**D**). $n = 15$ mice per group for neutrophil depletion; $n = 5$ mice per group for CD8 and CD4 depletion; $n = 10$ mice per group for NK depletion. Data shown are one representative of two independent experiments. Mean tumor volume (**E**) and survival curves (**F**) for mice inoculated with 5×10^5 4T1-Luc tumor cells in the mammary fat pad and treated as in **Fig. 1A**, with treatment starting 6 days after inoculation with surgical resection on day 15. In **E** and **F**, $n = 11$ for NSG untreated, $n = 13$ for NSG CIP, $n = 10$ for NOD/SCID untreated, and $n = 9$ for all other groups. Data are compiled from two independent experiments. Tumor growth data in **E** represent mean ± SEM. ****, $P < 0.0001$ by log-rank (Mantel–Cox) test. ns, not significant.

monotherapies at all time points (**Fig. 5B**). Granzyme production, measured by mean fluorescence intensity of the granzyme B^+ population, was also highest in the triple combination group (**Fig. 5B**). Similar prolonged activation of NK cells was observed in lung-infiltrating NK cells of E0771 tumor–bearing mice (Supplementary Fig. S10A–S10C). CIP treatment also led to an increase in the fraction of NK cells expressing PD-1 and increased the level of PD-1 expression (**Fig. 5C**; Supplementary Fig. S10D).

We next profiled the expression of activating receptors and cell death ligands on the surface of lung-infiltrating NK cells. Although a greater proportion of NK cells expressed the activating receptors DNAM-1 and NKG2D one day after treatment in the 4T1 model, this response was not exclusive to the CIP triple combination and was restricted to early time points, especially in the case of DNAM-1 (Supplementary Fig. S11A). In the E0771 model, NKG2D expression was sustained only in CIP-treated mice (Supplementary Fig. S11B). NK cells exert target cell killing not only through release of cytotoxic granules, but also through cell surface receptors in the form of death ligands FasL and TRAIL (5). In the 4T1-Luc model, no changes were noted in surface expression of FasL, and membrane TRAIL was expressed by similarly low fractions of the lung NK cells that received CIP treatment or were untreated (Supplementary Fig. S11C). Expression of both FasL and membrane TRAIL was more apparent in NK cells of E0771 tumor–bearing mice, and CIP treatment elevated surface expression of both death ligands (Supplementary Fig. S11D). Altogether, NK cells showed upregulation of multiple effector pathways in the lungs following CIP treatment, including sustained expression of granzyme B.

STING activation–driven type I IFN synergizes with IL2 to promote granzyme expression in NK cells

CDNs have a very short half-life *in vivo* (28) and hence we expected that CDNs were unlikely to directly stimulate STING in NK cells outside of the primary tumor. To measure direct uptake of CDNs by NK cells, we treated 4T1 tumor–bearing mice with CIP in the presence of a fluorophore-conjugated CDN. At 6 hours

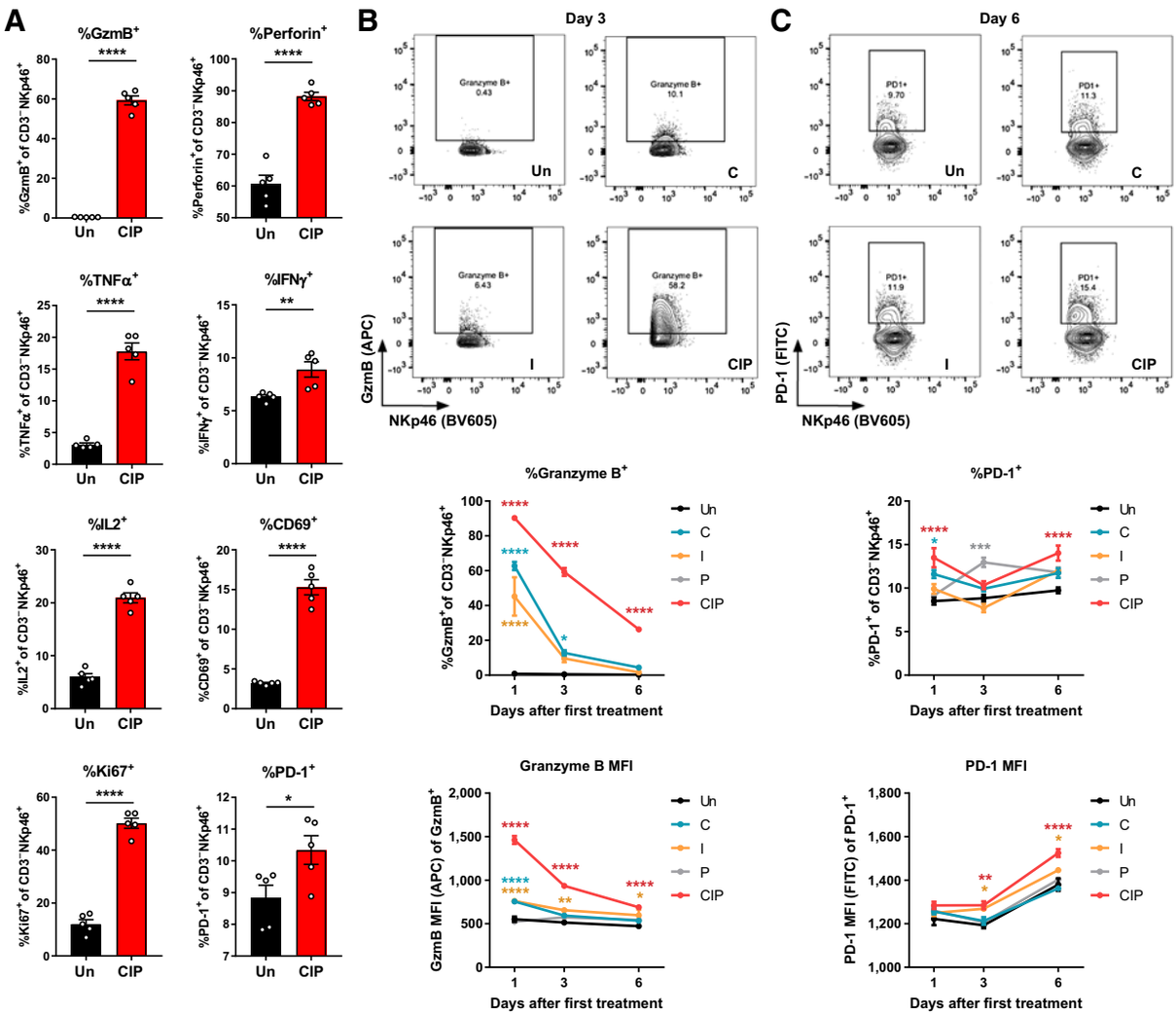

Figure 5.

NK cells are activated in the lungs in response to CIP immunotherapy. Balb/c mice were inoculated with 5×10^5 4T1-Luc tumor cells in the mammary fat pad and treated with CIP or individual agents as in **Fig. 1A** when tumors reached 50 to 100 mm^3. Lungs were isolated 1, 3, or 6 days after initiation of treatment, as indicated, and NK-cell functional markers quantified by flow cytometry. **A,** NK-cell expression of granzyme B, perforin, TNFα, IFNγ, IL2, CD69, Ki67, and PD-1 3 days post–treatment initiation. Representative flow cytometry plots, percentage of positive cells, and mean fluorescence intensity (MFI) for NK-cell expression of granzyme B (**B**) and PD-1 (**C**). Shown are mean ± SEM and are representative of two independent experiments ($n = 5$ animals/group per time point). *, $P < 0.05$; **, $P < 0.01$; ***, $P < 0.001$; ****, $P < 0.0001$ versus untreated at each time point by two-way ANOVA followed by Student *t* test (**A**) or Dunnett multiple comparisons test (**B** and **C**).

after treatment, a small proportion of $CD45^+$ cells in the primary tumor took up the labeled CDN. Among these leukocytes, a proportion of NK cells internalized the STING agonist (**Fig. 6A**). In the blood and lungs, no uptake of CDN by NK cells was detected (**Fig. 6B** and **C**). It therefore seemed unlikely that the intratumorally administered STING agonist is directly acting on lung-infiltrating NK cells. However, downstream of intratumoral STING activation is production of type I IFNs by host and/or tumor cells (8, 29). Utilizing IFNβ reporter mice expressing enhanced yellow fluorescent protein (eYFP) in the IFNβ locus, CIP treatment of E0771 tumor–bearing mice generated a larger fraction of tumor-resident $CD45^+$ cells expressing eYFP 24 hours after treatment in tumors compared with untreated controls (**Fig. 6D**). Similarly increased IFNβ production was not observed within the lungs, signifying that CDNs stimulate the majority of type I IFN cytokine secretion outside of the lung tissue (**Fig. 6E**). Examination of immune cells comprising the $eYFP^+$ population revealed neutrophils as the primary IFNβ producers within the tumor microenvironment and $CD11c^+$ DCs as IFNβ producers within the lungs (**Fig. 6D** and **E**). Apart from the tumor, elevated levels of type I IFNs and IFNγ were observed in the serum 6 and 24 hours after the first dose of CIP therapy (**Fig. 6F**), suggesting that circulating type I IFN synergizes with IL2 to induce the phenotypic changes observed in lung NK cells.

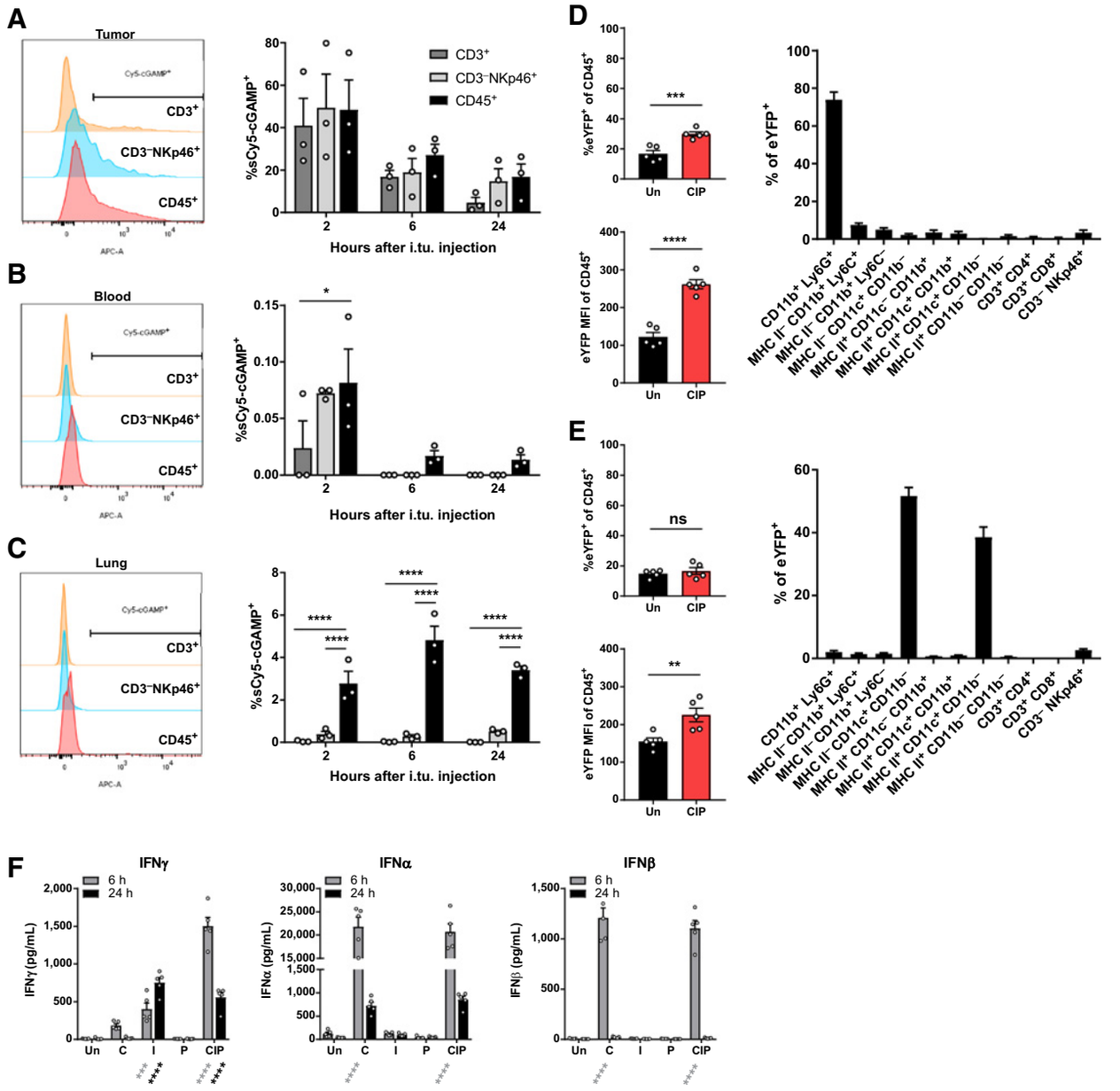

Figure 6.

Direct CDN uptake by NK cells is minimal and transient, whereas systemic IFNs are elevated with treatment. **A–C,** Balb/c mice were inoculated with 4T1-Luc cells in the mammary fat pad and treated intratumorally with a mixture of 30 μg 2′3′ c-di-AM(PS)$_2$ and 5 nmoles sulfo-Cy5 2′3′ c-GAMP in 30 μL and intraperitoneally with Alb-IL2 and anti–PD-1. Shown are representative Cy5 (APC) histograms (**A–C**, left) and fraction of cell types that are Cy5$^+$ in the tumor (**A**), blood (**B**), and lungs (**C**). Data shown are mean ± SEM and are representative of one independent experiment ($n = 3$ animals/group). **D** and **E,** IFNβ reporter mice were inoculated with E0771 cells in the mammary fat pad and treated with one dose of 30 μg 2′3′ c-di-AM(PS)$_2$ i.tu., 30 μg Alb-IL2 i.p., and 200 μg anti–PD-1 i.p. 2 weeks after tumor inoculation. A total of 24 hours after treatment, tumors (**D**) and lungs (**E**) were assessed for eYFP signal within the CD45$^+$ population. Fraction of CD45$^+$ cells expressing eYFP (top), eYFP MFI (bottom), and proportion of immune cell types within the eYFP$^+$ population are shown (right). Data represent mean ± SEM from one independent experiment ($n = 5$ animals/group). **F,** Balb/c mice inoculated with 4T1-Luc cells were treated as in **Fig. 1A**. Shown are serum cytokine levels 6 and 24 hours after one dose of CIP or indicated individual agents (**F**). Data shown are mean ± SEM and are representative of two independent experiments ($n = 5$ animals/group). *, $P < 0.05$; **, $P < 0.01$; ***, $P < 0.001$; ****, $P < 0.0001$ by two-way ANOVA followed by Dunnett multiple comparisons test versus CD45$^+$ (**A–C**) or versus untreated (**F**) or by two-tailed Student t test (**D** and **E**). ns, not significant.

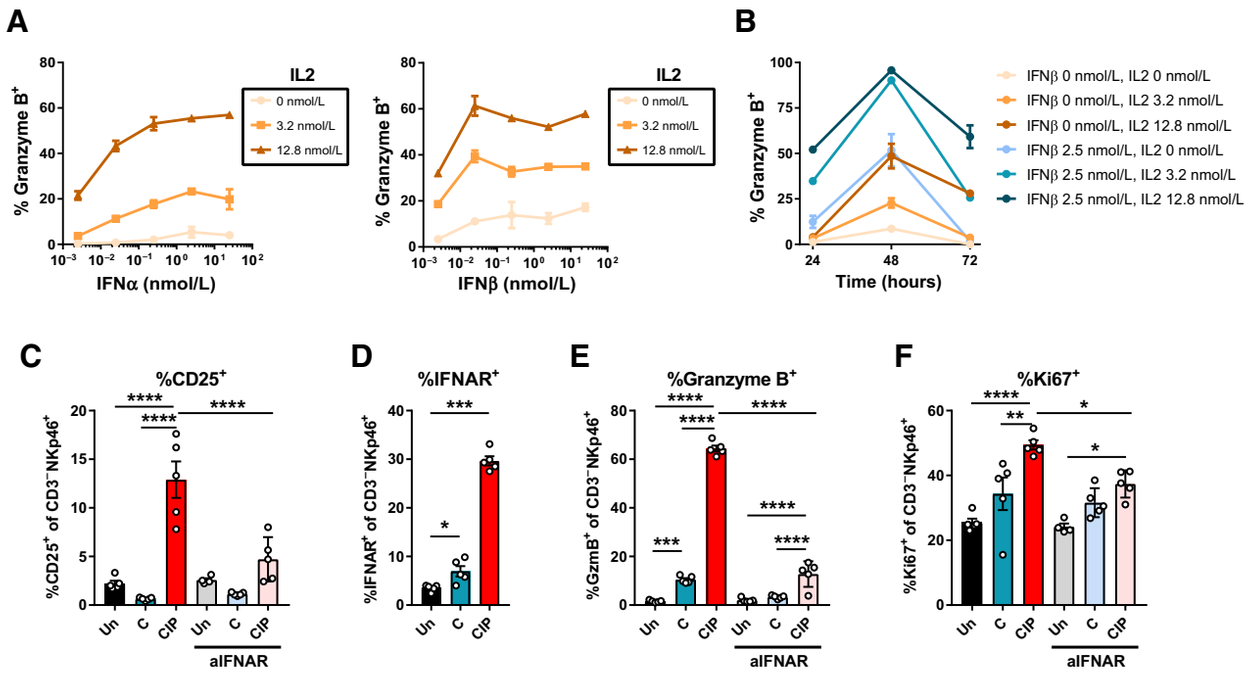

Figure 7.

IL2 and type I IFN synergistically promote sustained granzyme expression in NK cells. Purified NK cells were incubated *in vitro* with indicated doses of IL2 and IFNα or IFNβ for 24 hours, and granzyme expression was quantified by flow cytometry (**A**). Fraction of *in vitro* stimulated NK cells expressing granzyme B at 24, 48, and 72 hours after stimulation (**B**). **C–F,** Balb/c mice bearing 4T1 tumors were treated with 30 μg CDN, 30 μg Alb-IL2, and 200 μg anti-PD-1 in the presence or absence of an IFNAR-1 blocking antibody, and lungs were isolated 3 days after treatment for analysis of NK cells quantified by flow cytometry. Shown are percentages of NK cells expressing CD25 (**C**), IFNAR-1 (**D**), granzyme B (**E**), and Ki67 (**F**). Data shown are mean ± SEM and are representative of two independent experiments ($n = 5$ animals/group). *, $P < 0.05$; **, $P < 0.01$; ***, $P < 0.001$; ****, $P < 0.0001$ by two-way ANOVA followed by Tukey multiple comparisons test.

Consistent with this idea, titrated combinations of Alb-IL2 with IFNα or IFNβ generated synergistic, dose-dependent increases in the fraction of granzyme B–producing NK cells *in vitro*, mimicking the functional enhancements seen in NK cells *in vivo* (**Fig. 7A**). Sustained expression of granzyme B after stimulation *in vitro* with IFNβ and Alb-IL2 was also replicated (**Fig. 7B**).

To understand the source of this synergy between type I IFN and IL2, we dissected how combined stimulation of NK cells *in vivo* with CDN and Alb-IL2 changed surface receptor expression of IFNAR-1 and the high-affinity IL2 receptor. NK cells isolated from the lungs of mice 3 days after CIP treatment exhibited increased expression of both IL2Rα and IFNAR-1 that was not detected with CDN monotherapy (**Fig. 7C** and **D**). Blockade of IFNAR-1 by intraperitoneal anti–IFNAR-1 antibody prior to treatment with CIP significantly diminished NK-cell expression of CD25 (**Fig. 7C**). IFNAR-1 blockade also reduced the fraction of NK cells expressing granzyme B by approximately 80% to the baseline level induced by Alb-IL2 treatment alone (**Fig. 7E**). Blockade of IFNAR-1 signaling additionally reduced expression of TNFα and IFNγ in NK cells by nearly half and reduced the fraction of NK cells expressing NKG2D, but IFNAR-1 blockade did not significantly impact CIP-induced perforin expression (Supplementary Fig. S12A–S12D). In the absence of IFNAR-1 signaling, CIP immunotherapy no longer induced PD-1 surface expression on NK cells above the level of untreated controls (Supplementary Fig. S12E). Finally, IFNAR-1 blockade also lowered the expression of Ki67 in NK cells by around 25%, though some proliferation due to IL2 remained detectable in the anti–IFNAR-1 CIP group (**Fig. 7F**). In summary, CIP therapy promotes NK-cell activation through synergy between STING agonism–derived type I IFN and IL2.

Discussion

In this study, we report the use of intratumoral CDN STING agonist therapy combined with systemic extended half-life IL2 and anti–PD-1 checkpoint blockade as an effective means to potentiate long-term survival following neoadjuvant therapy in models of metastatic triple-negative breast cancer. STING agonist treatment is known to cause tumor vasculature collapse, resulting in an initial wave of hemorrhagic necrosis followed by rapid influx of innate immune cells, including neutrophils (13, 30). Such a vasculature damage–mediated response is consistent with our finding that early tumor control was unaffected by early lymphocyte depletion. Although CIP combination therapy controlled primary tumor growth on a short time scale, combining CIP with surgical resection greatly enhanced overall outcomes, with a majority of animals surviving long-term. Overall survival, unlike primary tumor growth, was dependent on host immunity. Notably, neoadjuvant administration of CIP was significantly superior to adjuvant treatment. Previous studies using the 4T1 model of metastatic breast cancer theorized that survival benefit in the neoadjuvant setting may be limited to therapies that invoke antitumor T-cell responses (31). Here, we found that NK cells, rather than T cells,

were critical for prevention of metastases, despite evidence of a tumor antigen–specific T-cell response. Inflammation resulting from wound healing induced by surgical intervention may inhibit T-cell control of preexisting metastases (32), and surgical stress may further cause NK-cell dysfunction through downregulation of NK-cell adhesion molecules CD62L and CD11b and decreased KLRG1 expression (33), potentially explaining the discrepancy observed between treatment in the neoadjuvant and adjuvant settings.

Clinically, NK cells have been implicated in metastasis immunosurveillance across multiple cancer types, with high NK-cell infiltration of tumors correlating with positive clinical outcomes (34). In patients with breast cancer, NK-cell genes NKp46, NKp30, NKG2D, CRTAM, DNAM-1, CD96, LFA-1, and CD1d—implicated in NK- and NKT-cell activation and adhesion—provide a predictive signature of recurrence-free survival (35). Meta-analysis of microarray data from human primary breast tumor samples finds that nearly all breast cancer subtypes express NKG2D and DNAM-1 ligands, though NK-cell inhibitory receptors become upregulated as cancer progresses (36, 37). The near ubiquity of these NK-activating ligands across breast tumors (38) in parallel with apparent dysfunction of NK cells, motivates the development of therapies that recruit NK cells to sites of metastasis and promote NK-cell activation as a treatment paradigm to clear metastases.

Precedent from preclinical studies has been established for the NK-cell–activating effects of STING agonists, IL2, and PD-1 checkpoint blockade individually. In the case of STING agonism, either endogenous tumor-derived 2′3′-cGAMP or exogenous administration of STING agonists leads to NK-mediated clearance of $CD8^+$ T-cell–resistant solid tumors lacking MHC I expression (14, 15). Chemoimmunotherapies featuring STING agonists are reliant, in part, on NK-cell activation (39). Finally, clearance of metastases following sustained release of perioperative CDNs was dependent on both NK- and T-cell responses (40). IL2 has long been documented as an essential signal for NK-cell maturation, proliferation, and survival (41). In the context of NK-cell antitumor immunity, IL2 and other common gamma chain cytokines can reinvigorate NK cells from anergic phenotypes (42). Finally, conflicting evidence exists surrounding the function of PD-1 as a putative exhaustion marker for NK cells (24, 43). Despite the uncertain role of PD-1 on NK cells, we observe a survival benefit when adding PD-1 checkpoint blockade antibody to CDN + Alb-IL2 (Supplementary Fig. S1A), likely due to modulation of both NK and T cells (44, 45). Beyond PD-1, blockade of alternative coinhibitory receptors merits further study to overcome surgery-induced NK- and T-cell dysfunction. For example, NK-specific checkpoint receptors, such as NKG2A, may be relevant to explore; disruption of this signaling pathway or others may prove more synergistic with CI than PD-1 blockade.

When combined, CIP immunotherapy agents induced prolonged expression of several NK-cell effector molecules, including granzyme B, perforin, TNFα, and to a lesser extent IFNγ, with an important role for CDN-induced type I IFN in this response (Supplementary Fig. S12F). *In vitro*, both type I IFNs and IL2 independently led to large proportions of NK cells expressing granzyme B; however, only the combination led to sustained granzyme production. In murine NK cells, granzyme B is regulated at the translational level, as resting NK cells have high levels of preexisting mRNA that can be further enhanced by cytokine stimulation (46). Following IFNα stimulation of splenocytes, *Gzmb* is also one of the most highly upregulated, STAT1-dependent genes differentiating wild type versus $STAT1^{-/-}$ mice (47, 48), genetically demonstrating the link between type I IFN signaling and granzyme B expression. Likewise, STAT5, downstream of IL2 and other common gamma chain–utilizing cytokines, is known to bind the *Gzmb* locus (49). Wiedemann and colleagues found in MCMV viral infection that *Gzmb* is one of the most highly downregulated genes after infection in STAT5-deficient NK cells, highlighting the importance of STAT5 in NK-cell cytotoxicity (50). NK cells deficient in CD25 also display impaired antiviral immunity (50). Further studies are needed to definitively determine the mechanisms mediating IFN/IL2 synergy in granzyme production.

Toxicity remains a key challenge in the clinical translation of many combination immunotherapies and is often poorly predicted by mouse models. However, early clinical trials of STING agonists combined with PD-1 blockade, as well as combinations of tumor-targeted IL2 and checkpoint blockade, have already proven to be safe, with few dose-limiting toxicities (44, 51). Combinations of the long half-life IL2 molecule Bempegaldesleukin with PD-1/PD-L1 blockade have also been demonstrated to be tolerable, induce T- and NK-cell expansion, and increase expression of genes associated with T- and NK-cell cytotoxicity (44). Given the striking therapeutic efficacy we demonstrate here with combined STING agonist/IL2/checkpoint blockade treatment in multiple orthotopic models of metastatic breast cancer, exploration of this combination in the clinic appears warranted.

Authors' Disclosures

D.J. Irvine reports personal fees from Elicio Therapeutics, Strand Therapeutics, Repertoire Immune Medicines, Ankyra Therapeutics, and Venn Therapeutics outside the submitted work. No disclosures were reported by the other authors.

Authors' Contributions

L.E. Milling: Conceptualization, data curation, formal analysis, validation, investigation, visualization, methodology, writing–original draft, writing–review and editing. **D. Garafola:** Investigation. **Y. Agarwal:** Investigation. **S. Wu:** Investigation. **A. Thomas:** Investigation. **N. Donahue:** Investigation. **J. Adams:** Investigation. **N. Thai:** Investigation. **H. Suh:** Resources. **D.J. Irvine:** Conceptualization, supervision, funding acquisition, writing–original draft, writing–review and editing.

Acknowledgments

This work was supported by the Marble Center for Nanomedicine; the Ragon Institute of MGH, MIT, and Harvard; and the Koch Institute Support (core) Grant P30-CA14051 from the NCI.

L.E. Milling is supported by the National Institute of General Medical Sciences Biotechnology Training Grant T32GM833430 and the Siebel Scholarship. D.J. Irvine is an investigator of the Howard Hughes Medical Institute. This work was supported by the Marble Center for Nanomedicine; the Ragon Institute of MGH, MIT, and Harvard; and the Koch Institute Support (core) Grant P30-CA14051 from the NCI. The authors thank the Koch Institute Swanson Biotechnology Center for technical support specifically the Preclinical Modeling, Imaging, & Testing Core facility and the flow cytometry facility. They also thank Emi Lutz and K. Dane Wittrup for producing the recombinant type I IFNs used in the *in vitro* NK stimulation assays.

The publication costs of this article were defrayed in part by the payment of publication fees. Therefore, and solely to indicate this fact, this article is hereby marked "advertisement" in accordance with 18 USC section 1734.

Note

Supplementary data for this article are available at Cancer Immunology Research Online (http://cancerimmunolres.aacrjournals.org/).

Received March 30, 2021; revised August 18, 2021; accepted October 20, 2021; published first October 22, 2021.

References

1. Moynihan KD, Irvine DJ. Roles for innate immunity in combination immunotherapies. Cancer Res 2017;77:5215–21.
2. Chang RB, Beatty GL. The interplay between innate and adaptive immunity in cancer shapes the productivity of cancer immunosurveillance. J Leukocyte Biol 2020;108:363–76.
3. Lee SC, Srivastava RM, López-Albaitero A, Ferrone S, Ferris RL. Natural killer (NK):dendritic cell (DC) cross talk induced by therapeutic monoclonal antibody triggers tumor antigen-specific T cell immunity. Immunol Res 2011;50:248–54.
4. Bald T, Krummel MF, Smyth MJ, Barry KC. The NK cell–cancer cycle: advances and new challenges in NK cell–based immunotherapies. Nat Immunol 2020;21: 835–47.
5. Myers JA, Miller JS. Exploring the NK cell platform for cancer immunotherapy. Nat Rev Clin Oncol 2021;18:85–100.
6. Moynihan KD, Opel CF, Szeto GL, Tzeng A, Zhu EF, Engreitz JM, et al. Eradication of large established tumors in mice by combination immunotherapy that engages innate and adaptive immune responses. Nat Med 2016;22:1402–10.
7. Zhu EF, Gai SA, Opel CF, Kwan BH, Surana R, Mihm MC, et al. Synergistic innate and adaptive immune response to combination immunotherapy with anti-tumor antigen antibodies and extended serum half-life IL-2. Cancer Cell 2015;27:489–501.
8. Corrales L, Glickman LH, McWhirter SM, Kanne DB, Sivick KE, Katibah GE, et al. Direct activation of STING in the tumor microenvironment leads to potent and systemic tumor regression and immunity. Cell Rep 2015;11:1018–30.
9. Wang-Bishop L, Wehbe M, Shae D, James J, Hacker BC, Garland K, et al. Potent STING activation stimulates immunogenic cell death to enhance antitumor immunity in neuroblastoma. J Immunother Cancer 2020;8:e000282.
10. Sivick KE, Desbien AL, Glickman LH, Reiner GL, Corrales L, Surh NH, et al. Magnitude of therapeutic STING activation determines CD8+ T cell-mediated anti-tumor immunity. Cell Rep 2018;25:3074–85.
11. Woo SR, Fuertes MB, Corrales L, Spranger S, Furdyna MJ, Leung MYK, et al. STING-dependent cytosolic DNA sensing mediates innate immune recognition of immunogenic tumors. Immunity 2014;41:830–42.
12. Dubensky TW, Kanne DB, Leong ML. Rationale, progress and development of vaccines utilizing STING-activating cyclic dinucleotide adjuvants. Ther Adv Vaccines 2013;1:131–43.
13. Francica BJ, Ghasemzadeh A, Desbien AL, Theodros D, Sivick KE, Reiner GL, et al. TNFalpha and radio-resistant stromal cells are essential for therapeutic efficacy of cyclic dinucleotide STING agonists in non-immunogenic tumors. Cancer Immunol Res 2018;6:422–33.
14. Nicolai CJ, Wolf N, Chang IC, Kirn G, Marcus A, Ndubaku CO, et al. NK cells mediate clearance of CD8+ T cell–resistant tumors in response to STING agonists. Sci Immunol 2020;5:eaaz2738.
15. Marcus A, Mao AJ, Lensink-Vasan M, Wang L, Vance RE, Raulet DH. tumor-derived cGAMP triggers a STING-mediated interferon response in non-tumor cells to activate the NK cell response. Immunity 2018;49:754–63.
16. Hagerling C, Gonzalez H, Salari K, Wang CY, Lin C, Robles I, et al. Immune effector monocyte–neutrophil cooperation induced by the primary tumor prevents metastatic progression of breast cancer. Proc Natl Acad Sci U S A 2019;116:21704–14.
17. Dent R, Trudeau M, Pritchard KI, Hanna WM, Kahn HK, Sawka CA, et al. Triple-negative breast cancer: clinical features and patterns of recurrence. Clin Cancer Res 2007;13:4429–34.
18. Pulaski BA, Ostrand-Rosenberg S. Mouse 4T1 breast tumor model. Curr Protoc Immunol 2001.
19. Jin C, Lagoudas GK, Zhao C, Bullman S, Bhutkar A, Hu B, et al. Commensal microbiota promote lung cancer development via γδ T cells. Cell 2019;176:998–1013.
20. Sivakumar PV, Garcia R, Waggie KS, Anderson-Haley M, Nelson A, Hughes SD. Comparison of vascular leak syndrome in mice treated with IL21 or IL2. Comparative Med 2013;63:13–21.
21. Assier E, Jullien V, Lefort J, Moreau JL, Santo JPD, Vargaftig BB, et al. NK cells and polymorphonuclear neutrophils are both critical for IL-2-induced pulmonary vascular leak syndrome. J Immunol 2004;172:7661–8.
22. Ishikawa H, Ma Z, Barber GN. STING regulates intracellular DNA-mediated, type I interferon-dependent innate immunity. Nature 2009;461:788–92.
23. Waldmann TA. The biology of interleukin-2 and interleukin-15: implications for cancer therapy and vaccine design. Nat Rev Immunol 2006;6:595–601.
24. Hsu J, Hodgins JJ, Marathe M, Nicolai CJ, Bourgeois-Daigneault MC, Trevino TN, et al. Contribution of NK cells to immunotherapy mediated by PD-1/PD-L1 blockade. J Clin Invest 2018;128:4654–68.
25. Bosma MJ, Carroll AM. The scid mouse mutant: definition, characterization, and potential uses. Annu Rev Immunol 1991;9:323–50.
26. Shultz LD, Ishikawa F, Greiner DL. Humanized mice in translational biomedical research. Nat Rev Immunol 2007;7:118–30.
27. Scrimieri F, Askew D, Corn DJ, Eid S, Bobanga ID, Bjelac JA, et al. Murine leukemia virus envelope gp70 is a shared biomarker for the high-sensitivity quantification of murine tumor burden. Oncoimmunology 2013;2:e26889.
28. Wehbe M, Wang-Bishop L, Becker KW, Shae D, Baljon JJ, He X, et al. Nanoparticle delivery improves the pharmacokinetic properties of cyclic dinucleotide STING agonists to open a therapeutic window for intravenous administration. J Control Release 2021;330:1118–29.
29. Demaria O, Gassart AD, Coso S, Gestermann N, Domizio JD, Flatz L, et al. STING activation of tumor endothelial cells initiates spontaneous and therapeutic antitumor immunity. Proc Natl Acad Sci U S A 2015;112: 15408–13.
30. Weiss JM, Guérin MV, Regnier F, Renault G, Galy-Fauroux I, Vimeux L, et al. The STING agonist DMXAA triggers a cooperation between T lymphocytes and myeloid cells that leads to tumor regression. Oncoimmunology 2017;6: e1346765.
31. Liu J, Blake SJ, Yong MCR, Harjunpää H, Ngiow SF, Takeda K, et al. Improved efficacy of neoadjuvant compared to adjuvant immunotherapy to eradicate metastatic disease. Cancer Discov 2016;6:1382–99.
32. Krall JA, Reinhardt F, Mercury OA, Pattabiraman DR, Brooks MW, Dougan M, et al. The systemic response to surgery triggers the outgrowth of distant immune-controlled tumors in mouse models of dormancy. Sci Transl Med 2018;10: eaan3464.
33. Tai LH, Souza CT de, Bélanger S, Ly L, Alkayyal AA, Zhang J, et al. Preventing postoperative metastatic disease by inhibiting surgery-induced dysfunction in natural killer cells. Cancer Res 2013;73:97–107.
34. López-Soto A, Gonzalez S, Smyth MJ, Galluzzi L. Control of metastasis by NK cells. Cancer Cell 2017;32:135–54.
35. Ascierto ML, Idowu MO, Zhao Y, Khalak H, Payne KK, Wang XY, et al. Molecular signatures mostly associated with NK cells are predictive of relapse free survival in breast cancer patients. J Transl Med 2013;11:145.
36. Mamessier E, Sylvain A, Thibult ML, Houvenaeghel G, Jacquemier J, Castellano R, et al. Human breast cancer cells enhance self tolerance by promoting evasion from NK cell antitumor immunity. J Clin Invest 2011;121:3609–22.
37. Mamessier E, Sylvain A, Bertucci F, Castellano R, Finetti P, Houvenaeghel G, et al. Human breast tumor cells induce self-tolerance mechanisms to avoid NKG2D-mediated and DNAM-mediated NK cell recognition. Cancer Res 2011; 71:6621–32.
38. Diefenbach A, Jamieson AM, Liu SD, Shastri N, Raulet DH. Ligands for the murine NKG2D receptor: expression by tumor cells and activation of NK cells and macrophages. Nat Immunol 2000;1:119–26.
39. Wang F, Su H, Xu D, Dai W, Zhang W, Wang Z, et al. Tumour sensitization via the extended intratumoural release of a STING agonist and camptothecin from a self-assembled hydrogel. Nat Biomed Eng 2020;4:1090–101.
40. Park CG, Hartl CA, Schmid D, Carmona EM, Kim HJ, Goldberg MS. Extended release of perioperative immunotherapy prevents tumor recurrence and eliminates metastases. Sci Transl Med 2018;10:eaar1916.
41. Henney CS, Kuribayashi K, Kern DE, Gillis S. Interleukin-2 augments natural killer cell activity. Nature 1981;291:335–8.
42. Ardolino M, Azimi CS, Iannello A, Trevino TN, Horan L, Zhang L, et al. Cytokine therapy reverses NK cell anergy in MHC-deficient tumors. J Clin Invest 2014; 124:4781–94.
43. Judge SJ, Dunai C, Aguilar EG, Vick SC, Sturgill IR, Khuat LT, et al. Minimal PD-1 expression in mouse and human NK cells under diverse conditions. J Clin Invest 2020;130:3051–68.
44. Diab A, Tannir NM, Bentebibel S-E, Hwu P, Papadimitrakopoulou V, Haymaker C, et al. Bempegaldesleukin (NKTR-214) plus nivolumab in patients with advanced solid tumors: phase I dose-escalation study of safety, efficacy, and immune activation (PIVOT-02). Cancer Discov 2020; 10:1158–73.
45. Sharma M, Khong H, Fa'ak F, Bentebibel SE, Janssen LME, Chesson BC, et al. Bempegaldesleukin selectively depletes intratumoral Tregs and potentiates T cell-mediated cancer therapy. Nat Commun 2020;11:661.
46. Fehniger TA, Cai SF, Cao X, Bredemeyer AJ, Presti RM, French AR, et al. Acquisition of murine NK cell cytotoxicity requires the translation of a pre-existing pool of granzyme B and perforin mRNAs. Immunity 2007;26: 798–811.

47. Zimmerer JM, Lesinski GB, Radmacher MD, Ruppert A, Carson WE. STAT1-dependent and STAT1-independent gene expression in murine immune cells following stimulation with interferon-alpha. Cancer Immunol Immunother 2007;56:1845–52.
48. Lee CK, Rao DT, Gertner R, Gimeno R, Frey AB, Levy DE. Distinct requirements for IFNs and STAT1 in NK cell function. J Immunol 2000; 165:3571–7.
49. Villarino AV, Sciumè G, Davis FP, Iwata S, Zitti B, Robinson GW, et al. Subset- and tissue-defined STAT5 thresholds control homeostasis and function of innate lymphoid cells STAT5 function in innate lymphocytes. J Exp Medicine 2017;214: 2999–3014.
50. Wiedemann GM, Grassmann S, Lau CM, Rapp M, Villarino AV, Friedrich C, et al. Divergent role for STAT5 in the adaptive responses of natural killer cells. Cell Rep 2020;33:108498.
51. Meric-Bernstam F, Sandhu SK, Hamid O, Spreafico A, Kasper S, Dummer R, et al. Phase Ib study of MIW815 (ADU-S100) in combination with spartalizumab (PDR001) in patients (pts) with advanced/metastatic solid tumors or lymphomas. J Clin Oncol 37, 2019 (suppl; abstr 2507).